PCCP

Accepted Manuscript

ROYAL SOCIETY OF CHEMISTRY

www.rsc.org/pccp

PCCP

ARTICLE

Utilizing alkoxyphenyl substitutents for side-chain engineering of efficient benzo[1,2-*b*:4,5-*b*']dithiophene-based small molecule organice solar cells

Received 00th January 20xx,
Accepted 00th January 20xx

DOI: 10.1039/x0xx00000x

www.rsc.org/

Zhengkun Du[a,c], Weichao Chen[a], Meng Qiu[a], Yanhua Chen[a,b], Ning Wang[a], Ting Wang[a], Mingliang Sun[b], Donghong Yu*[c,d], and Renqiang Yang*[a]*

A new two-dimensional (2D) conjugated small molecule, namely DCA3TBDTP, with alkoxyphenyl substituted benzo[1,2-*b*:4,5-*b*']dithiophene (BDT) unit as the central core, octyl cyanoacetate as the end-capped groups and terthiophene as the π-linked bridge, was designed and synthesized for solution-processed organic solar cells (OSCs) as electron donor material, in which alkoxyphenyl group was introduced as a weak electron-donating side chain of the BDT moiety. The DCA3TBDTP molecule exhibited good solubility, deep highest occupied molecular orbital (HOMO) level (-5.25 eV), appropriate optical band-gap (1.82 eV) and high decomposition temperature (362 °C). By applying the simple solution spin-coating fabrication process, bulk heterojunction (BHJ) OSCs based on DCA3TBDTP and [6,6]-phenyl-C_{61}-butyric acid methyl ester ($PC_{61}BM$) exhibited decent power conversion efficiency (PCE) of 4.51% with a high open-circuit voltage (V_{oc}) of 0.90 V when thermal annealing at only 70 °C.

Introduction

Sparked by a report from Chen *et al.* in 2011[1], benzo[1,2-*b*:4,5-*b*'] dithiophene (BDT, as the core) based acceptor-donor-acceptor (A-D-A) small molecule organic solar cells (SMOSC) reached its power conversion efficiency (PCE) of 5.44%, which was mainly contributed by BDT's large and rigid planar structure as a structural analogue of electron-rich anthracene moiety with enhanced electron delocalization and promoted cofacial π-π stacking in the solid state, thus being favored by charge transport in OSC devices[2-5]. This had made it a star electron-donating unit in high-performance conjugated donor materials in SMOSCs with their promisingly comparable PCEs (exceeding 9%) to their polymer counterparts[6-8], possessing great advantages of relatively simple synthesis, purification and well-defined structures thus less batch-to-batch variation, possible versatile structural design thus easier control of energy levels, and high charge carrier mobilities[9,10]. Since then, significant progress on such BDT based SMOSCs have been achieved by both incorporating a series of dye building blocks as various acceptor motifs such as 3-ethulrodanine[11], indenedione (1,3-indandione)[12], 1,3-dimethylbarbituric acid[9], and DPP[13], as well as by symmetrical π-conjugated substitutions on phenyl unit of BDT's with alkylthienyl[14], alkylphenyl[15], alkylsilylethynyl[16] and alkylselenophene[17] groups. Such π-conjugated substituents in the orthogonal direction of BDT results in 2-dimensional (2D) expanded delocalization of π-electrons to the conjugated side groups thus better interchain π- π stacking, which could benefits exciton diffusion and charge transport, in comparison to 1D BDT units substituted with non-conjugated side groups like dialkoxy[11] or dialkylthiol[6] substituents, therefore improved broad light absorbance and deep highest occupied molecular orbital (HOMO) energy levels which could contribute to relatively high open-circuit voltage (V_{oc}) (ca. 0.90-1.0 V) and high efficiency (PCE > 7%)[6,18].

State-of-art altering side chain structures on BDT moiety has presented great ability in fine tuning such electronic properties as energy levels, bandgap, and charge carrier mobility, etc.[6,18]. Among the vast variety of developed BDT-based electron-donating derivatives, systematic investigations on 1D alkyl-, alkoxy-, and alkylthiol-BDT based SMOSCs had been explored by Chen *et. al.* in a series of paper: the choice of weaker electron-donating ability of alkylthiol- than alkoxy-BDT based SMOSC leading a V_{oc} of 0.91 V[6]; the replace of strong electron donor 2-ethylhexyloxy side chain on BDT unit with a less electron-donating octyl side chain resulting even lower HOMO energy level (-5.02 eV) and thus a much higher V_{oc} (0.98 V)[19]. However, for 2D π-conjugated units attached BDT in SMOSCs, only strong electron donors like alkylthiophene, alkylbenzene, alkylselenophene, and alkylsilylethyne[14-17] had been reported. In order to systematically engineer such side

[a] CAS Key Laboratory of Bio-based Materials, Qingdao Institute of Bioenergy and Bioprocess Technology, Chinese Academy of Sciences, Qingdao 266101, China.
[b] Institute of Materials Science and Engineering, Ocean University of China, Qingdao 266100, China.
[c] Department of Chemistry and Bioscience, Aalborg University, DK-9220, Aalborg, Denmark.
[d] Sino-Danish Centre for Education and Research (SDC), Niels Jensens Vej 2, DK-8000, Aarhus, Denmark.
Electronic Supplementary Information (ESI) available. See
DOI: 10.1039/x0xx00000x

chain dependency, the promising less strong alkoxylphenyl substituents ought to be taken into considerations for the molecular design. Such alkoxyphenyl side group has been recently pioneered by 2-dimensional BDT based polymer from both Zou's group with PBDTPO-DTBO[20] and ours with PBDTPF-DTBT[21] (with fluorinated alkoxyphenyl side chain), which demonstrated respectively high PCE of 6.2% and 7.02%, and the mobility up to 0.22 and 0.034 $cm^2/(V{\cdot}s)$. Meanwhile, we designed and synthesized a new small molecule BDT-PO-DPP by replacing the alkoxyl groups in BDT unit with alkoxyphenyl ones for extended conjugation along the side chain directions and gave a PCE of 5.63% after thermal annealing at 110 °C[22]. In order to systematically explore the molecular structure dependency on electronic properties like energy level and charge mobility, further design of more SMOSCs based on alkoxyphenyl substituted BDT would be fundamentally essential. On the other hand, being one of the widely used end-capped blocks for building high-performance SMOSCs due to its simple conjugated structure and strong electron-withdrawing ability, octyl cyanoacetate could not only effectively regulate the energy levels of the HOMO and lowest unoccupied molecular orbital (LUMO) but also greatly improve the solubility of the targeted small molecules[1,9,11-13,18].

Considering the above discussions, in this work, for side-chain engineering of BDT based high PCE SMOSCs, we introduced the weak electron-donating group *para*-alkoxyphenyl as aromatic substituent on BDT to obtain a new 2D conjugated small molecule DCA3TBDTP (Scheme **1**). This compound consists of three segments: octyl cyanoacetate as the end-capped groups, terthiophene as the π-linked bridge and alkoxyphenyl substituted BDT as the central core. The molecule DCA3TBDTP exhibited excellent solubility in common organic solvents and good thermal stability, and DCA3TBDTP/$PC_{61}BM$ blend film showed a hole mobility up to 2.74×10^{-4} $cm^2/(V{\cdot}s)$, which was measured *via* the space-charge limit current (SCLC) model. BHJ-OSCs fabricated with DCA3TBDTP as donor and $PC_{61}BM$ as acceptor showed a decent PCE of 4.51% with a high open-circuit voltage of 0.90 V after thermal annealing at low temperature 70 °C.

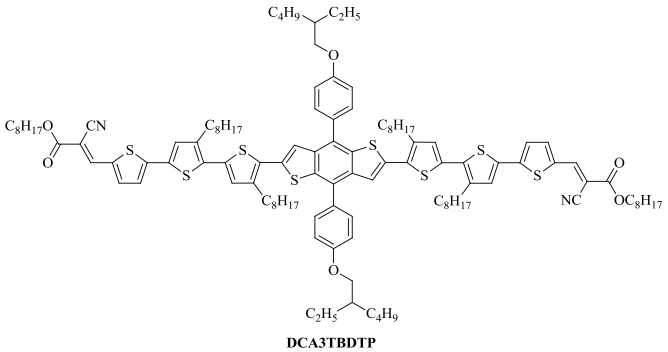

Scheme 1. Chemical structure of DCA3TBDTP.

Experimental section

Materials

All chemicals, unless otherwise specified, were purchased from commercial sources and used as received. Toluene and tetrahydrofuran (THF) were freshly distilled at the presence of sodium and benzophenone under nitrogen prior to use. 5''-Bromo-4',4''-dioctyl-2,2':5',2''-trithiophene-5-carbaldehyde (**6**) was synthesized as reported in the literature[23].

Instruments and measurements

Nuclear magnetic resonance (NMR) spectra were taken on a Bruker AVANCE-III 600 Spectrometer. High resolution mass spectra (HRMS) were recorded under APCI mode on a Bruker Maxis UHRTOF spectrometer. Thermal gravimetric analysis (TGA) measurements were performed on STA-409 at a heating rate of 10 °C/min. The differential scanning calorimetry (DSC) analysis was carried on Perkin Elmer diamond differential scanning calorimeter. UV-vis absorption spectra were recorded with a PerkinElmer Lambda 25 spectrophotometer. Cyclic voltammetry (CV) was performed using a CHI660D electrochemical workstation with a glassy carbon working electrode, a saturated calomel reference electrode (SCE), and a platinum wire counter electrode at a scan rate of 50 mV/s. Tetrabutylammonium phosphorus hexafluoride (Bu_4NPF_6, 0.1 M) in acetonitrile was used as the supporting electrolyte. Surface roughness and morphology of thin films of active layers were characterized by atomic force microscopy (AFM) on an Agilent 5400 working at the tapping mode. X-ray diffraction (XRD) pattern was recorded on a Bruker D8 Advance.

Fabrication and characterization of organic solar cells

Photovoltaic devices were fabricated on pre-patterned indium tin oxide (ITO) coated glass substrates with the device geometry of ITO/PEDOT:PSS/DCA3TBDTP:$PC_{61}BM$/Ca(10 nm)/Al(100 nm). The ITO glass substrates were cleaned ultrasonically in acetone, toluene, methanol and isopropyl alcohol sequentially. And then, oxygen plasma treatment was processed for 20 min, spin-coated with PEDOT:PSS at 4000 rpm, and dried under argon for 30 min at 160 °C. The photosensitive layer was prepared by spin-coating a blend solution of the DCA3TBDTP and $PC_{61}BM$ with a weight ratio of 3:1, 2:1 or 1:1 in deoxygenated anhydrous chloroform on the ITO/PEDOT:PSS substrate in a glove box. The thickness of active layer films measured by a Dektak 150 profilometer was around 100 nm. Finally, Ca (10 nm) and aluminum (100 nm) were thermally evaporated and deposited on the top of active layer in a defined area of 0.1 cm^2 at a vacuum of ~2×10^{-4} Pa. The current density-voltage (*J-V*) characteristics were recorded with a Keithley 2420 source measurement under AM 1.5G illumination (100 mW/cm^2) from a Newport solar simulator. A standard silicon solar cell was used to calibrate the light intensity. The external quantum efficiencies (EQE) of the OSCs were measured using a certified Newport incident photon conversion efficiency (IPCE) measurement system.

Synthesis

The synthetic routes of the targeted small molecule are presented in the Scheme **2**.

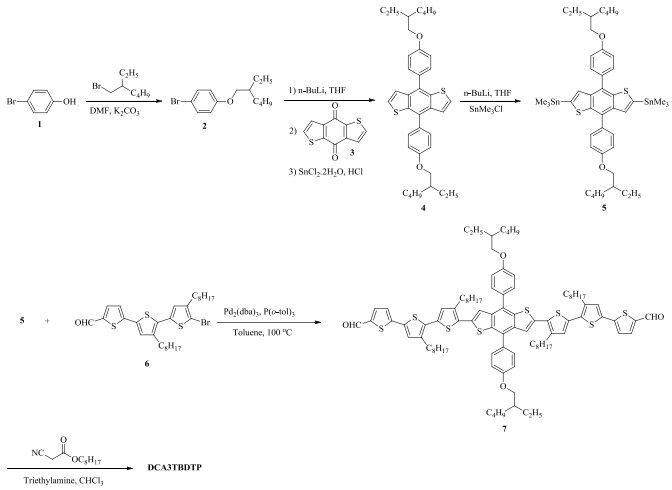

Scheme 2. Synthetic routes for DCA3TBDTP.

1-Bromo-4-(2'-ethylhexyloxy)benzene (2). Under argon atmosphere, 4-bromophenol (5.20 g, 30 mmol) and K_2CO_3 (4.98 g, 36 mmol) was added into 100 mL DMF in a two-neck flask. After stirring for 5 min, 2-ethylhexyl bromide (6.75 g, 35 mmol) was added *via* a syringe. The mixture was heated to 120 °C for 24 h in darkness. The cooled mixture was poured into water and then extracted with diethyl ether three times. The combined organic phase was dried over anhydrous magnesium sulfate ($MgSO_4$). After removing the organic solvents, the residue was purified on a silica gel column eluting with petroleum ether. Compound **2** was obtained as pale yellow oil (7.53 g, 90% yield). ^{1}H NMR (600 MHz, $CDCl_3$): δ (ppm): 7.36 (d, 2H), 6.78 (d, 2H), 3.80 (d, 2H), 1.70 (m, 1H), 1.51-1.28 (m, 8H), 0.93-0.89 (m, 6H). ^{13}C NMR (150 MHz, $CDCl_3$): δ (ppm): 158.52, 132.15, 116.34, 112.46, 70.78, 39.32, 30.49, 29.06, 23.83, 23.04, 14.08, 11.09.

4,8-bis(4-ethylhexyloxy-1-phenyl)-benzo[1,2-*b*:4,5-*b*']dithiophene (4). In a 200 mL argon purged three-neck flask, *n*-BuLi (15 mL, 1.6 M in hexane) was added dropwise into a solution of **2** (6.85 g, 24 mmol) in THF (50 mL) at -78 °C. The mixture was kept at -78 °C for 1.5 h. Subsequently, benzo[1,2-*b*:4,5-*b*']dithiophene-4,8-dione (1.76 g, 8 mmol) was added quickly, and the mixture was stirred for 3 h at 55 °C. After cooling to room temperature, a solution of $SnCl_2{\cdot}2H_2O$ (14.45 g, 64 mmol) in 10% HCl (25.6 mL) was added and then the mixture was stirred for an additional 2.5 h at 55 °C. The mixture was quenched with 60 mL of deionized water and then extracted with diethyl ether. The combined organic extract was dried with anhydrous $MgSO_4$ and evaporated the solvent under vacuum. The residue was purified via a silica gel column using petroleum ether as eluent to obtain compound **4** as a white solid (1.82 g, 38% yield). ^{1}H NMR (600 MHz, $CDCl_3$): δ (ppm): 7.62 (d, 4H), 7.38 (d, 2H), 7.34 (d, 2H), 7.09 (d, 4H), 3.96 (d, 4H), 1.80 (m, 2H), 1.60-1.36 (br, 16H), 0.98 (t, 6H), 0.94 (t, 6H). ^{13}C NMR (150 MHz, $CDCl_3$): δ (ppm): 159.25, 138.30, 136.24, 131.41, 130.50, 130.01, 126.99, 123.09, 114.74, 70.57, 39.49, 30.61, 29.15, 23.94, 23.10, 14.13, 11.19.

2,6-Bis(trimethyltin)-4,8-bis(4-ethylhexyloxy-1-phenyl)-benzo[1,2-*b*:4,5-*b*']dithio-phene (5). In a 100 mL argon purged flask, *n*-BuLi (3.25 mL, 1.6 M in hexane) was added into dry THF solution (45 mL) of compound **4** (1.20 g, 2 mmol) at 0 °C. After the addition, the mixture was kept at room temperature for 1.5 h, and then the $SnMe_3Cl$ (5.75 mL, 1.0 M in hexane) was added quickly *via* a syringe at 0 °C. The mixture was stirred overnight at room temperature. Subsequently, the mixture was poured into deionized water (40 mL) and extracted with diethyl ether three times. The combined organic phase was dried over anhydrous $MgSO_4$. After removing the organic solvents, the residue was recrystallized from acetone to afford the yellow solid compound **5** (1.10 g, 60% yield). ^{1}H NMR (600 MHz, $CDCl_3$): δ (ppm): 7.64 (d, 4H), 7.38 (s, 2H), 7.10 (d, 4H), 3.97 (d, 4H), 1.80 (m, 2H), 1.60-1.36 (br, 16H), 0.99 (t, 6H), 0.94 (t, 6H), 0.35 (t, 18H). ^{13}C NMR (150 MHz, $CDCl_3$): δ (ppm): 159.05, 142.59, 141.62, 137.07, 132.06, 130.86, 130.57, 128.45, 114.64, 70.49, 39.54, 30.63, 29.17, 23.96, 23.11, 14.14, 11.22, -8.36.

Synthesis of compound (7). In a 100 mL well flame-dried flask, compound **6** (0.76 g, 1.32 mmol) and **5** (0.55 g, 0.6 mmol) were dissolved in anhydrous toluene (25 mL). After the solution being degassed with argon three times, $Pd_2(dba)_3$ (16 mg, 0.018 mmol) and P(*o*-tol)$_3$ (32 mg, 0.108 mmol) were added under argon protection quickly. The reaction mixture was slowly heated to 100 °C for 36 h under argon atmosphere. The cooled mixture was poured into deionized water and extracted with $CHCl_3$ three times. The combined organic phase was dried over anhydrous $MgSO_4$ and concentrated under vacuum. The crude residue was purified via silica gel column using petroleum/CH_2Cl_2 (v/v, from 1:1 to 1:5) as eluent to obtain compound **7** (0.64 g, 67% yield) as a red solid. ^{1}H NMR (600 MHz, $CDCl_3$), δ (ppm): 9.85 (s, 2H), 7.68 (d, 4H), 7.66 (d, 2H), 7.36 (s, 2H), 7.21 (d, 2H), 7.18 (s, 2H), 7.11 (d, 4H), 7.00 (s, 2H), 3.97 (d, 4H), 2.77 (m, 8H), 1.81 (m, 2H), 1.69-1.61 (m, 8H), 1.53-1.23 (m, 56H), 0.99 (t, 6H), 0.94 (t, 6H), 0.88-0.85 (m, 12H). ^{13}C NMR (150 MHz, $CDCl_3$), δ (ppm): 182.43, 159.40, 146.97, 141.52, 141.32, 140.93, 138.49, 137.42, 136.78, 136.25, 134.26, 133.41, 132.60, 131.68, 130.97, 130.41, 129.42, 129.35, 129.14, 123.98, 121.45, 114.86, 70.61, 39.52, 31.89, 31.85, 30.60, 30.37, 29.53, 29.51, 29.47, 29.41, 29.39, 29.29, 29.23, 29.17, 23.93, 23.10, 22.69, 22.66, 14.13, 14.11, 11.19.

Synthesis of DCA3TBDTP. Under argon atmosphere, octyl cyanoacetate (0.55 g, 2.8 mmol) was added to a stirred chloroform solution (30 mL) of triethylamine (0.05 mL) and compound **7** (0.40 g, 0.25 mmol) *via* a syringe at 28 °C. The solution was stirred at 28 °C for 40 hours under argon, then was added with water (35 ml) and extracted with $CHCl_3$ three times. The organic phase was dried over anhydrous $MgSO_4$ and the solvent was removed under vacuum. The crude product was purified by means of column chromatography over silica gel using petroleum/CH_2Cl_2 (v/v, 1:2) as eluent and then recrystallized in mixing solvent of methanol/chloroform to obtain DCA3TBDTP (0.35 g, 72% yield) as a black solid. ^{1}H NMR

(600 MHz, $CDCl_3$), as found in Figure S3, δ (ppm): 8.25 (d, 2H), 7.68 (d, 4H), 7.64 (d, 2H), 7.37 (s, 2H), 7.23 (s, 2H), 7.20 (d, 2H), 7.12 (d, 4H), 7.01 (d, 2H), 4.29 (t, 4H), 3.97 (d, 4H), 2.77 (m, 8H), 1.81 (m, 2H), 1.75 (m, 4H), 1.70-1.61 (m, 8H), 1.53-1.23 (m, 76H), 0.99 (t, 6H), 0.94 (t, 6H), 0.90-0.85 (m, 18H). ^{13}C NMR (150 MHz, $CDCl_3$), δ (ppm): 163.11, 159.41, 147.32, 146.17, 141.36, 141.15, 139.33, 138.49, 136.79, 136.23, 134.23, 134.17, 133.09, 131.81, 130.96, 130.41, 129.59, 129.42, 129.41, 124.14, 121.48, 116.12, 114.86, 97.48, 70.61, 66.59, 39.52, 31.89, 31.85, 31.78, 30.60, 30.58, 30.37, 29.53, 29.48, 29.39, 29.29, 29.23, 29.19, 29.17, 29.16, 28.57, 25.81, 23.93, 23.10, 22.69, 22.65, 14.13, 14.12, 14.10, 11.19. MS (UHR-TOF): calcd. for $C_{118}H_{156}N_2O_6S_8$ $[M]^+$: 1952.9729; found: 1952.9724.

Result and discussion

Synthesis and characterization

The detailed synthetic routes of the small molecule DCA3TBDTP are outlined in Scheme **2**. Compound **5** and **6** were synthesized according to reported procedures[20,23]. The important precursor **7** containing two aldehyde groups was synthesized by a Stille coupling reaction between compound **5** and **6**. The target small molecule DCA3TBDTP was obtained by means of Knoevenagel condensation between octyl cyanoacetate and the corresponding aldehyde compound **7**. The purity of the targeted compound for the device fabrication was guaranteed by multiple column chromatographic purification and recrystallization in mixing solvent of methanol/chloroform. The targeted compound was fully characterized with HRMS, ^{1}H and ^{13}C NMR (Figure **S3**). The DCA3TBDTP shows a good solubility in common organic solvents, which is a prerequisite for solution processed SMOSCs.

Thermal stability

The thermal property of DCA3TBDTP was investigated through TGA and DSC. As shown in Figure **1**, DCA3TBDTP exhibited a good thermal stability with a decomposition temperature (T_d, 5% weight loss) at 362 °C under nitrogen atmosphere, evidencing sufficient thermal stability for its device application. As exhibited in Figure **S1**, the first thermal heating scan (heat **1** curve) was applied for cancelling the history of thermal/solvent induced crystallization of the sample. Thermodynamic phase transition temperatures including melting point and crystallization temperature were adopted from the second heating scan and cooling of the thermogram (heat **2** and cooling curve). Distinct melting peaks from both solvent induced (heat **1**) and thermally crystalized (heat **2**) samples reveal the formation of their crystal structure and therefore indicate the strong intermolecular interactions among the small molecules via π-π stacking within the aromatic moieties and hydrophobic interactions within the alkyl side chains. It is found that the main melting endotherm of DCA3TBDTP occurred at 192.84 °C and the corresponding melting enthalpy (ΔH_m) calculated from the integrated area of melting peak was 39.96 J/g. During the cooling process, the DCA3TBDTP showed a crystallization ΔH_m of 23.75 J/g at 180.87 °C, proving that the small molecule has an obvious tendency to crystallize[24]. While the larger enthalpy value of solvent induced crystallization (ΔH_m of 44.80 J/g) announces higher degree of crystallinity than that of the materials crystalized via cooling, indicating possibly good phase separation between donor DCA3TBDTP and acceptor $PC_{61}BM$ caused by solvent evaporation during spin-coating the active layer materials.

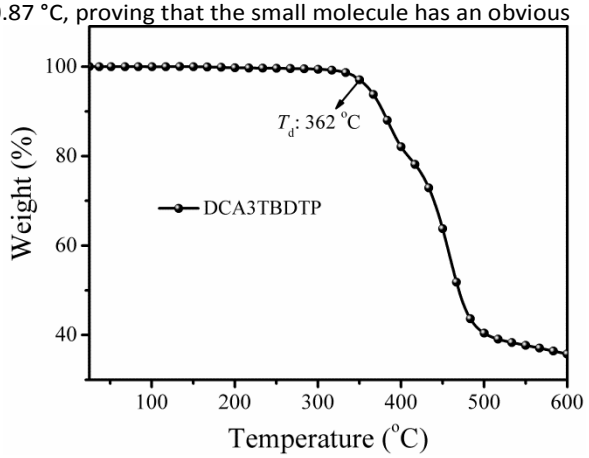

Figure 1. TGA curve of DCA3TBDTP with a heating rate of 10 °C /min under nitrogen atmosphere.

Optical properties

Figure **2** explored the normalized ultraviolet-visible (UV-vis) absorption of DCA3TBDTP in dilute chloroform solution (5×10^{-6} mol/L) and in thin film. The UV-vis absorption spectrum of DCA3TBDTP in solution exhibited an absorption peak at 500 nm with the maximum molar extinction coefficient (ε_{max}) of 8.68×10^4 L/(mol·cm) (Figure **S2**), arising from intramolecular charge-transfer (ICT) between the donor and acceptor moieties. The shoulder peak ranging from 350-450 nm can be attributed to the π-π* transitions of the conjugated units, The DCA3TBDTP thin film showed broader absorption across the visible region (300-700 nm) due to more effective electron push-pull effects and extended π-π packing of the molecular backbones in solid state. Compared with that in solution, the thin film absorption peak displayed a bathochromic shift of about 73 nm, indicating strong intermolecular π-π interaction

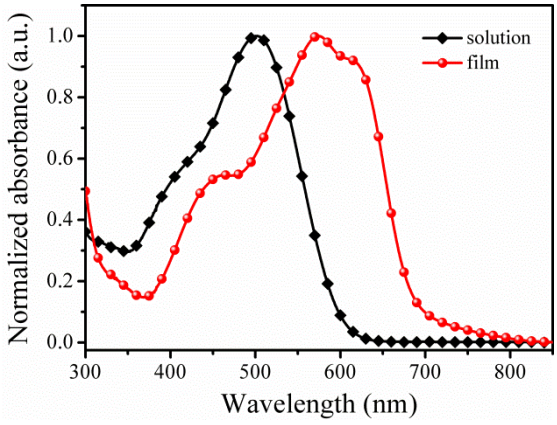

Figure 2. Normalized UV-vis absorption spectra of DCA3TBDTP in $CHCl_3$ solution and in thin film.

and aggregation in the solid state due to improved planar construction of the 2D side chains. The optical band gap (ΔE_g^{opt}) of DCA3TBDTP is estimated to be 1.82 eV derived from the absorption onset of thin film (683 nm). In terms of OSC design, such low band gap of DCA3TBDTP will lead to higher photocurrent, making this molecule more useful for OSC applications.

Electrochemical properties

The electrochemical properties of DCA3TBDTP were investigated by cyclic voltammetry (CV). A solution of tetrabutylammonium phosphorus hexafluoride (Bu_4NPF_6, 0.1 M) in acetonitrile was used as the supporting electrolyte and the potential scan rate was 50 mV/s. As shown in Figure **3a**, DCA3TBDTP displayed one reversible oxidation wave. The redox potential of the Fc/Fc^+ internal reference is 0.39 V vs SCE. The HOMO energy level of the target molecule was determined by the empirical formula of $E_{HOMO} = - e(E_{Ox} + 4.8 – E_{1/2,(Fc/Fc^+)})$. The onset oxidation potential of DCA3TBDTP is 0.84 V, thus the corresponding HOMO energy level is -5.25 eV. Additionally, the LUMO energy level of DCA3TBDTP, calculated from the HOMO and optical band gap, is -3.43 eV.

The energy level diagrams of DCA3TBDTP and other materials used in the solution-processed BHJ SMOSCs are shown in Figure **3b**. The LUMO energy level offset (ΔE_{LUMO}) and HOMO energy level offset (ΔE_{HOMO}) of DCA3TBDTP/$PC_{61}BM$ are 0.48 eV and 0.68 eV, respectively. The relatively unmatched ΔE_{LUMO} and ΔE_{HOMO} values could lead to an unbalanced charge dissociation[25], which is not conducive to the improvement of J_{sc}.

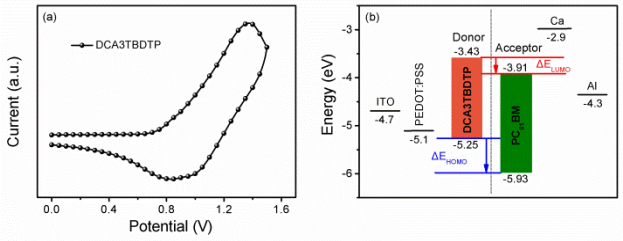

Figure 3. (a) Cyclic voltammogram of DCA3TBDTP thin film at a scan rate of 50 mV/s. (b) Energy level diagrams of DCA3TBDTP and other materials used in SM-OSCs.

Geometry and electronic structure

Density functional theory (DFT) was employed to investigate the electronic structure of the molecule DCA3TBDTP with B3LYP method at the 6-31G(d) basis set level in gas phase (Figure **4**), and the DFT calculation was performed by the Gaussian 09 program[26-29]. All the alkyl side chains were replaced with methyl groups to reduce the computational cost. The optimized molecular structure was confirmed to be in a stable local minimum of the ground state potential energy surface since there is no imaginary frequency by vibrational calculation at the same level of theory. The DFT-derived HOMO and LUMO energy levels of the molecule DCA3TBDTP were -5.10 eV and -2.91 eV, respectively. As shown in Figure **4**, the DCA3TBDTP presented a good planarity in the molecular backbone direction. However, the pendant benzene rings on the benzodithiophene of DCA3TBDTP exhibited a torsion angle of about 59.1° because of the space steric effect, leading to a relatively poor planarity in the side chain direction[22].

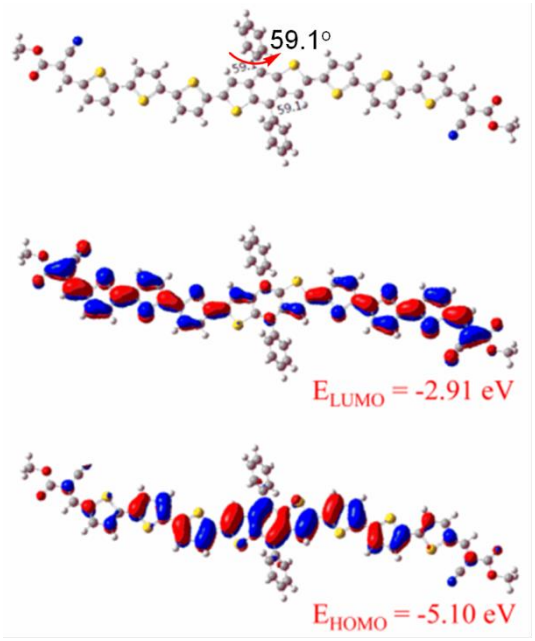

Figure 4. Optimized molecular geometry and frontier molecular orbitals (isovalue surface 0.02 au) using DFT evaluated with B3LYP method at the 6-31G(d) basis set level.

Photovoltaic properties

BHJ photovoltaic devices were fabricated with a conventional architecture of ITO/PEDOT:PSS/DCA3TBDTP:$PC_{61}BM$/Ca/Al, and tested under a simulated AM 1.5G illumination (100 mW/cm^2). Firstly, the blends of the DCA3TBDTP and $PC_{61}BM$ at different weight ratios were used to optimize the device performance. The detailed device parameters were summarized in Table **1**. With an increase of the DCA3TBDTP/$PC_{61}BM$ blend ratio from 1:1 to 3:1, V_{oc} had no obviously change. However, the short circuit current density (J_{sc}) firstly increased from 5.40 mA/cm^2 to 6.95 mA/cm^2 and then decreased to 6.22 mA/cm^2. Compared with the V_{oc} and J_{sc}, fill factor (FF) had been gradually increased. As is known to all, thermal annealing of the blend film could generally enhance the photovoltaic performance due to the improved morphology of active layer. Therefore, thermal annealing in the range of 50-90 °C was also employed to further optimize the device performance. With increasing annealing temperature, the values of J_{sc} and FF increased significantly compared to the pristine ones. Interestingly, the V_{oc} of BHJ solar cells remained almost constant before and after thermal annealing, as high as ~0.90 V which is similar with that of other reported BDT-based SMOSCs and is believed to be related to the deep HOMO (-5.25 eV) energy level of molecule

DCA3TBDTP (Figure **3b**)[6,11,23]. The current density versus voltage (*J*-*V*) curves of the optimized devices before and after thermal annealing at 70 °C was shown in Figure **5a**. Finally, a PCE of 4.51% for DCA3TBDTP-based small molecule OSC was obtained with a V_{oc} of 0.90 V, a J_{sc} of 7.88 mA/cm^2 and a FF of 63.66%, when the device was fabricated with a donor-acceptor weight ratio of 2:1 after thermal annealing at 70 °C.

Table 1. Photovoltaic performance of SMOSCs based on DCA3TBDTP/$PC_{61}BM$ with different blend ratios, under AM 1.5G illumination (100 mW/cm^2)

DCA3TBDTP/$PC_{61}BM$ (w:w)	Thermal annealing[a]	V_{oc} (V)	J_{sc} (mA/cm^2)	*FF* (%)	PCE_{max} (PCE_{ave})[b] (%)
1:1	no	0.89	5.40	42.40	2.04 (1.95)
2:1	no	0.89	6.95	61.88	3.83 (3.72)
3:1	no	0.90	6.22	62.22	3.48 (3.29)
2:1	50 °C	0.90	7.21	63.09	4.09 (3.97)
2:1	70 °C	0.90	7.88	63.66	4.51 (4.43)
2:1	90 °C	0.88	6.47	64.74	4.34 (4.20)

[a] Thermal annealing for 10 min. [b] Average value from ten devices.

To further understand the photo-to-electron conversion efficiencies of the DCA3TBDTP-based solar cells in the UV-vis region, the EQE curves of the optimized BHJ devices based on DCA3TBDTP/$PC_{61}BM$ (w:w, 2:1) are presented in Figure **5b**. The EQE curves pronounce a broad response covering 300-700 nm, consistent with the absorption spectrum. It is worth pointing out that thermal annealing improved the photo-response of active layer in whole range, leading to an increased J_{sc}. The J_{sc} (6.92 mA/cm^2 and 7.86 mA/cm^2) were calculated from integration of the EQE curves, which were consistent well with the J_{sc} (6.95 mA/cm^2 and 7.88 mA/cm^2) obtained from the *J*-*V* measurements before and after thermal annealing at 70 °C for the DCA3TBDTP/$PC_{61}BM$ (w:w, 2:1) devices.

Morphology and structural (X-ray) characterization

The atomic force microscopy (AFM) and transmission electron microscopy (TEM) are utilized to study the morphologies and phase separations of DCA3TBDTP/$PC_{61}BM$ (w:w, 2:1) blend films before and after thermal annealing at 70 °C. The active layer is spin-coated from $CHCl_3$ solution on glass/ITO/PEDOT:PSS substrate for AFM measurements. The corresponding topography and phase images are shown in Figure **6** (a, b-pristine films and d, e-thermal annealing films). Both the blend films before and after thermal annealing claimed a uniform and smooth surface, ensuring a better contact with the Ca/Al electrode and being helpful in the increase of the charge collection efficiency. The root mean square (RMS) roughness is *ca.*1.48 nm and 1.04 nm for pristine film and thermal annealing blend film, respectively. The decreased RMS suggested that the quality of DCA3TBDTP/$PC_{61}BM$ blend film could be improved by the thermal annealing. As shown in TEM images (Figure **6c** and **6f)**, thermal annealing blend film exhibits a better interpenetrating network containing slightly larger nanoscale phase separation in active layer. After annealing at 70 °C, the domain boundary intensity obviously reduced, which would decrease the trap state density existing in the boundary. Therefore, the transport and collection of the carrier charge was improved and the recombination current was also reduced. This is probably an important reason for the enhancement of J_{sc} and FF after thermal annealing in this work[23,30-33].

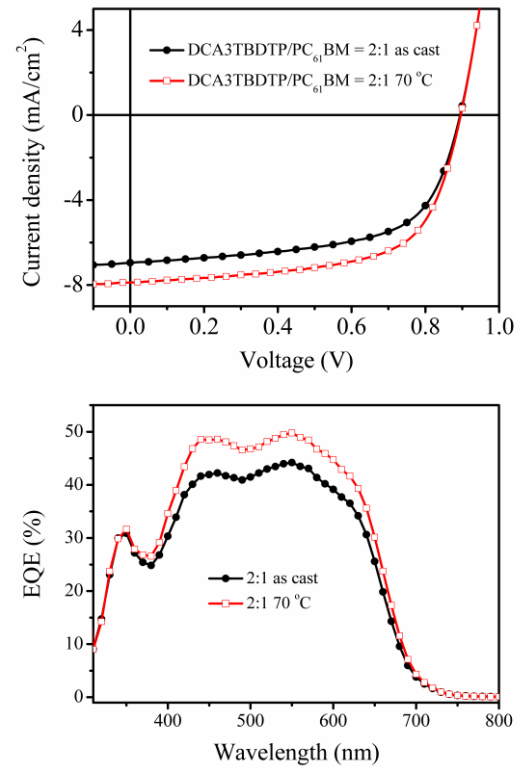

Figure 5. (a) *J-V* characteristics and (b) EQE curves of devices based on DCA3TBDTP/$PC_{61}BM$ (2:1, w/w) before and after thermal annealing at 70 °C.

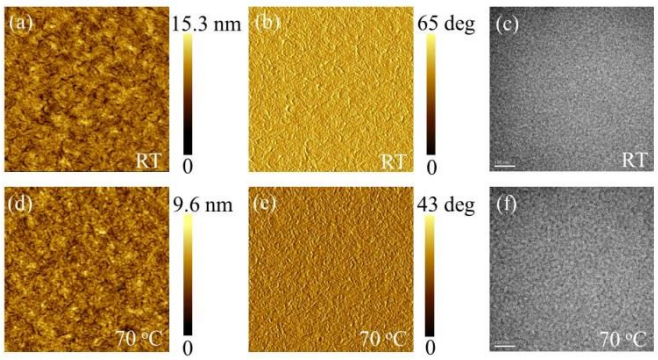

Figure 6. Tapping-mode AFM height (a, d) and phase (b, e) images (4 μm × 4 μm) and TEM images (c, f) of DCA3TBDTP/$PC_{61}BM$ (2:1, w/w) blend films before and after thermal annealing at 70 °C, scale bar: 100 nm.

To further understand the relationship between the photovoltaic performance and the annealing temperature, the crystallinity of DCA3TBDTP/$PC_{61}BM$ blend film before and after thermal annealing at 70 °C was investigated by X-ray diffraction (XRD). As shown in Figure **7**, the first-order diffraction peak at 2θ = 3.97° corresponding to the (100) lattice plane of the DCA3TBDTP with d_{100}-spacing value of 22.2 Å and the second-order diffraction peak (200) at 2θ = 7.94° was also clearly observed. The d_{100}-spacing is the distance between the main conjugated chains of the small molecules, separated by their side chains. The highly intense (100) diffraction peaks is resulted from many alkyl side chains around the main chain, which were featured by the solution-processed small molecules as reported[1,18]. Therefore the presence of these diffraction peaks indicated that the blend film exhibited an obvious ordered arrangement before and after thermal annealing. However, compared with the pristine film, the intensity of the diffraction peak of annealing film was significantly enhanced and the half-band width was also narrowed, indicating that the ordered arrangement and

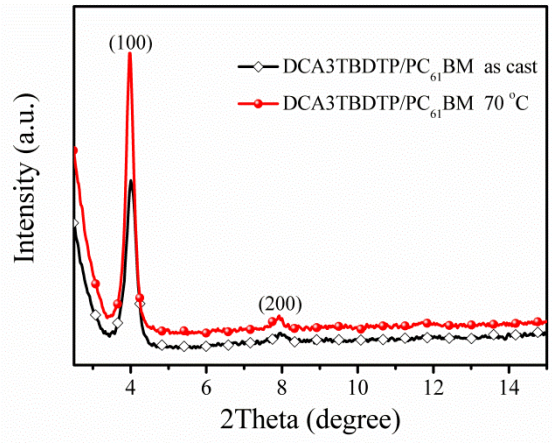

Figure 7. XRD patterns of DCA3TBDTP/$PC_{61}BM$ films spin-coated from $CHCl_3$ solution before and after thermal annealing at 70 °C.

degree of crystallinity was further improved in the active layer after thermal annealing[23,32]. This is also under a good agreement with the DSC results formerly discussed. The enhanced crystallinity underwent with stronger π-π stacking ability after thermal annealing could improve the carrier mobility which is beneficial to the carrier transport and collection, resulting in an improved J_{sc} and FF[31,32,34].

Hole mobility

The hole mobility of DCA3TBDTP/$PC_{61}BM$ blend film before and after thermal annealing at 70 °C was explored by the space-charge-limited current (SCLC) model[35] using a device configuration of ITO/PEDOT:PSS/DCA3TBDTP:$PC_{61}BM$ (2:1, 100 nm)/Au (Figure **8)**. The calculated hole mobility values of blend films were 1.34×10^{-4} $cm^2/(V\cdot s)$ and 2.74×10^{-4} $cm^2/(V\cdot s)$ before and after thermal annealing, respectively. The results indicated that thermal annealing contributes to the hole mobility improvement, which was another important factor for the enhanced device performance after thermal annealing at relatively low temperature.

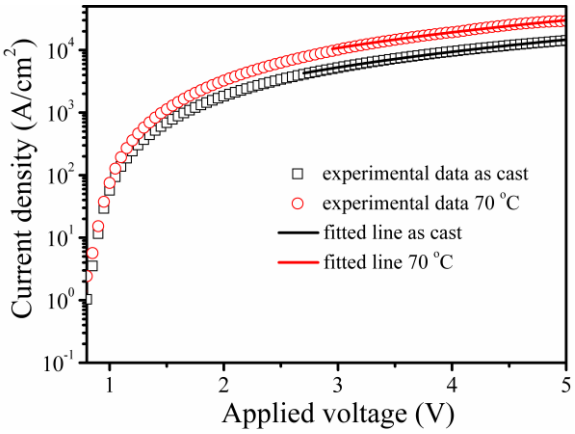

Figure 8. Current density (*J*)-voltage (*V*) curves for DCA3TBDTP based devices (the symbols are experimental data for hole transport, and the lines are fitted according to the space-charge-limited-current model).

Conclusion

A new small molecule DCA3TBDTP based on alkoxyphenyl substituted benzo[1,2-*b*:4,5-*b*']dithiophene, terthiophene and octyl cyanoacetate was designed and synthesized by Stille coupling and Knoevenagel reactions. The small molecule exhibited good thermal stability, solubility and deep HOMO energy level. As weak electron donor, alkoxylphenyl group as conjugated side chain was introduced into the molecular backbone without obvious influence on the optical band gap and crystallinity. Solution-processed organic solar cells based on DCA3TBDTP and $PC_{61}BM$ exhibited a PCE of 4.51% with a high V_{oc} of 0.90 V after thermal annealing at only 70 °C. The

encouraging results reveal that alkoxyphenyl substituted benzo[1,2-*b*:4,5-*b*']dithiophene derivative is a prospective two-dimensional heterocyclic core in constructing donor-acceptor type small molecules for high-efficiency solution-processed organic solar cells.

AUTHOR INFORMATION

Corresponding Author

*E-mail: yu@bio.aau.dk (D.Y.)
*E-mail: mlsun@ouc.edu.cn (M.S.)
*Fax: +86-532-80662778; Tel: +86-532-80662700. E-mail: yangrq@qibebt.ac.cn (R.Y.)

Acknowledgements

This work was supported by the National Natural Science Foundation of China (21204097, 21274134, 51173199, 51303197 and 61405209), the Ministry of Science and Technology of China (2014CB643501, 2010DFA52310), the Danish National Research Foundation, and Qingdao Municipal Science and Technology Program (11-2-4-22-hz and 14-2-4-28-jch). The work was carried out in the Danish Chinese Centre of Organic based Photovoltaics with Morphological Control. Support from the Sino-Danish Centre for Education and Research (SDC) is also fully acknowledged.

Notes and references

1 Y. S. Liu, X. J. Wan, F. Wang, J. Y. Zhou, G. K. Long, J. G. Tian and Y. S. Chen, *Adv. Mater.*, 2011, **23**, 5387.
2 S. C. Price, A. C. Stuart, L. Q. Yang, H. X. Zhou and W. You, *J. Am. Chem. Soc.*, 2011, **133**, 4625.
3 H. Y. Chen, J. H. Hou, S. Q. Zhang, Y. Y. Liang, G. W. Yang, Y. Yang, L. P. Yu, Y. Wu and G. Li, *Nat. Photonics*, 2009, **3**, 649.
4 Y. Y. Liang and L. P. Yu, *Acc. Chem. Res.*, 2010, **43**, 1227.
5 L. J. Huo, J. H. Hou, S. Q. Zhang, H. Y. Chen and Y. Yang, *Angew. Chem. Int. Ed.*, 2010, **49**, 1500.
6 B. Kan, Q. Zhang, M. M. Li, X. J. Wan, W. Ni, G. K. Long, Y. C. Wang, X. Yang, H. R. Feng and Y. S. Chen, *J. Am. Chem. Soc.*, 2014, **136**, 15529.
7 Z. C. He, C. M. Zhong, S. J. Su, M. Xu, H. B. Wu and Y. Cao, *Nat. Photonics*, 2012, **6**, 591.
8 Y. H. Liu, J. B. Zhao, Z. K. Li, C. Mu, W. Ma, H. W. Hu, K. Jiang, H. R. Lin, H. Ade and H. Yan, *Nat. Commun.*, 2014, **5**, DOI: 10.1038/ncomms6293.
9 Y. S. Chen, X. J. Wan and G. Long, *Acc. Chem. Res.*, 2013, **46**, 2645.
10 Y. Z. Lin, Y. F. Li and X. W. Zhan, *Chem. Soc. Rev.*, 2012, **41**, 4245.
11 J. Y. Zhou, X. J. Wan, Y. S. Liu, Y. Zuo, Z. Li, G. K. He, G. K. Long, W. Ni, C. X. Li, X. C. Su and Y. S. Chen, *J. Am. Chem. Soc.*, 2012, **134**, 16345.
12 S. L. Shen, P. Jiang, C. He, J. Zhang, P. Shen, Y. Zhang, Y. P. Yi, Z. J. Zhang, Z. B. Li and Y. F. Li, *Chem. Mater.*, 2013, **25**, 2274.
13 Y. Z. Lin, L. C. Ma, Y. F. Li, Y. Q. Liu, D. B. Zhu and X. W. Zhan, *Adv. Energy Mater.*, 2013, **3**, 1166.
14 D. Deng, Y. J. Zhang, L. Yuan, C. He, K. Lu and Z. X. Wei, *Adv. Energy Mater.*, 2014, **4**, DOI: 10.1002/aenm.201400538.
15 W. Ni, X. J. Wan, M. M. Li, Y. C. Wang and Y. S. Chen, *Chem. Commun.*, 2015, **51**, 4936.
16 N. Lim, N. Cho, S. Paek, C. Kim and J. K. Lee, *Chem. Mater.*, 2014, **26**, 2283.
17 Y. J. Kim, J. Y. Baek, J. J. Ha, D. S. Chung, S. K. Kwon, C. E. Park and Y. H. Kim, *J. Mater. Chem. C*, 2014, **2**, 4937.
18 J. Y. Zhou, Y. Zuo, X. J. Wan, G. K. Long, Q. Zhang, W. Ni, Y. S. Liu, Z. Li, G. K. He, C. X. Li, B. Kan, M. M. Li and Y. S. Chen, *J. Am. Chem. Soc.*, 2013, **135**, 8484.
19 W. Ni, M. M. Li, X. J. Wan, H. R. Feng, B. Kan, Y. Zuo and Y. S. Chen, *RSC Adv.*, 2014, **4**, 31977.
20 J. Yuan, L. Xiao, B. Liu, Y. F. Li, Y. H. He, C. Y. Pan and Y. P. Zou, *J. Mater. Chem. A*, 2013, **1**, 10639.
21 W. C. Chen, Z. K. Du, L. L. Han, M. J. Xiao, W. F. Shen, T. Wang, Y. H. Zhou and R. Q. Yang, *J. Mater. Chem. A*, 2015, **3**, 3130.
22 Z. K. Du, W. C. Chen, S. G. Wen, S. L. Qiao, Q. Liu, D. Ouyang, N. Wang, X. C. Bao and R. Q. Yang, *ChemSusChem*, 2014, **7**, 3319.
23 Z. K. Du, W. C. Chen, Y. H. Chen, S. L. Qiao, X. C. Bao, S. G. Wen, M. L. Sun, L. L. Han and R. Q. Yang, *J. Mater. Chem. A*, 2014, **2**, 15904.
24 Q. C. Yu, W. F. Fu, J. H. Wan, X. F. Wu, M. M. Shi and H. Z. Chen, *ACS Appl. Mater. Interfaces*, 2014, **6**, 5798.
25 J. H. Huang, X. Wang, X. Zhang, Z. X. Niu, Z. H. Lu, B. Jiang, Y. X. Sun, C. L. Zhan and J. N. Yao, *ACS Appl. Mater. Interfaces*, 2014, **6**, 3853.
26 M. J. Frisch, G. W. Trucks, H. B. Schlegel, G. E. Scuseria, M. A. Robb, J. R. Cheeseman, G. Scalmani, V. Barone, B. Mennucci, G. A. Petersson, H. Nakatsuji, M. Caricato, X. Li, H. P. Hratchian, A. F. Izmaylov, J. Bloino, G. Zheng, J. L. Sonnenberg, M. Hada, M. Ehara, K. Toyota, R. Fukuda, J. Hasegawa, M. Ishida, T. Nakajima, Y. Honda, O. Kitao, H. Nakai, T. Vreven, J. A. Montgomery, J. E. Jr. Peralta, F. Ogliaro, M. Bearpark, J. J. Heyd, E. Brothers, K. N. Kudin, V. N. Staroverov, T. Keith, R. Kobayashi, J. Normand, K. Raghavachari, A. Rendell, J. C. Burant, S. S. Iyengar, J. Tomasi, M. Cossi, N. Rega, J. M. Millam, M. Klene, J. E. Knox, J. B. Cross, V. Bakken, C. Adamo, J. Jaramillo, R. Gomperts, R. E. Stratmann, O. Yazyev, A. J. Austin, R. Cammi, C. Pomelli, J. W. Ochterski, R. L. Martin, K. Morokuma, V. G. Zakrzewski, G. A. Voth, P. Salvador, J. J. Dannenberg, S. Dapprich, A. D. Daniels, O. Farkas, J. B. Foresman, J. V. Ortiz, J. Cioslowski and D. J. Fox, Gaussian 09 revision b.01, Gaussian, Inc. Wallingford, CT, 2010.
27 C. T. Lee, W. T. Yang and R. G. Parr, *Phys. Rev. B*, 1988, **37**, 785.
28 A. D. Becke, *J. Chem. Phys.*, 1993, **98**, 5648.
29 W. J. Hehre, R. Ditchfield and J. A. Pople, *J. Chem. Phys.*, 1972, **56**, 2257.
30 H. Y. Wang, F. Liu, L. J. Bu, J. Gao, C. Wang, W. Wei and T. P. Russell, *Adv. Mater.*, 2013, **25**, 6519.
31 W. L. Leong, G. C. Welch, J. Seifter, J. H. Seo, G. C. Bazan and A. J. Heeger, *Adv. Energy Mater.*, 2013, **3**, 356.
32 L. M. Chen, Z. R. Hong, G. Li and Y. Yang, *Adv. Mater.*, 2009, **21**, 1434.
33 G. D. Wei, S. Y. Wang, K. Sun, M. E. Thompson and S. R. Forrest, *Adv. Energy Mater.*, 2011, **1**, 184.
34 J. Liu, H. Choi, J. Y. Kim, C. Bailey, M. Durstock and L. M. Dai, *Adv. Mater.*, 2012, **24**, 538.
35 V. D. Mihailetchi, J. Wildeman and P. W. M. Blom, *Phys. Rev. Lett.*, 2005, **94**, 126602.

Table of Contents:

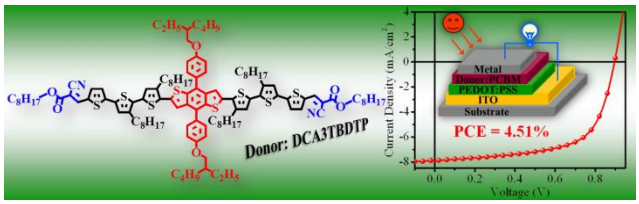

A new alkoxyphenyl substituted benzo[1,2-*b*:4,5-*b*']dithiophene-based small molecule was designed and synthesized for solution-processed organic solar cells.